Thermal Conductivity Accumulation in Amorphous Materials

Jason M. Larkin[1] and Alan J. H. McGaughey[1]

[1]*Department of Mechanical Engineering*

Carnegie Mellon University

Pittsburgh, PA 15213

(Dated: August 9, 2013)

Abstract

By definition, phonons are non-localized propagating vibrations that transport energy over distances much larger than the atomic spacing. For amorphous solids, with the exception of very long-wavelength (low-frequency) modes, the vibrational modes are non-propagating. Recently, experimental measurements of the thermal conductivity of amorphous materials demonstrate that propagating (phonon-like) modes with large mean free paths contribute significantly to thermal transport in amorphous materials.[1,2] Using broadband frequency domain thermal-reflectance, Regner et al. measured how the thermal conductivity of a-SiO_2 and a-Si thin films change with the penetration depth associated with the heating laser pulse.[1] Regner et al. argue that their measurements probe the mean free paths of propagating vibrational modes to measure the thermal conductivity accumulation function. Using lattice dynamics calculations and molecular dynamics simulations on realistic models of a-SiO_2 and a-Si, we predict and characterize the contributions from propagating and non-propagating vibrations to thermal conductivity. The vibrational mean free paths and (for the first time) the thermal conductivity accumulation functions are predicted for a-SiO_2 and a-Si and compared with experimental results of Regner et al. and varying thin film measurements. For a-SiO_2, the propagating modes are found to contribute negligibly for both bulk and thin films. We demonstrate the scaling of the low-frequency propagating mode diffusivities using (to our knowledge) the largest model of bulk a-Si. For a-Si, the propagating modes contribute significantly to thermal transport. We consider two scalings of the propagating mode diffusivities to compare with the results of Regner et al. and thin film measurements and find good qualitative agreement for both. Further experiments are suggested based on our predictions and the comparisons.

I. INTRODUCTION

The vibrational modes in disordered solids (i.e., alloys, amorphous materials) can be classified as propagons (propagating, i.e. phonon-like), diffusons (non-propagating, de-localized), and locons (non-propagating, localized).[3,4] Diffusons are de-localized but non-propagating, and contribute to thermal conductivity by coupling with other modes due to the disorder. Locons are localized and non-propagating, and do not contribute to thermal transport.

Experimental measurements and estimates based on experiments have demonstrated that propagating modes contribute significantly for amorphous silicon (a-Si) and[1,5–7] amorphous silicon nitride,[2] but not amorphous silica (a-SiO_2).[1,8–10] Notably, using broadband frequency domain thermal-reflectance, Regner et al. measured how the thermal conductivity of a-SiO_2 and a-Si thin films change with the penetration depth associated with the heating laser pulse.[1] Following the suggestion of Koh and Cahill, they interpret the measured value at a given penetration depth to be representative of the phonons with mean free path (MFP) less than that value, allowing for the construction of the so-called thermal conductivity accumulation function.[11–13] For a-SiO_2, the thermal conductivity of a 1000 nm film did not vary for penetration depths between 57 and 960 nm, suggesting that any propagating modes that contribute to thermal conductivity have MFPs below 57 nm. For a-Si, they find the thermal conductivities of thin films between 500 and 2000 nm vary by about 40% for penetration depths between 44 and 968 nm, suggesting that propagating modes with MFPs of 100 to 1000 nm contribute significantly to thermal conductivity.[1]

To understand the results of Regner et al. requires knowledge of the MFPs of the propagating modes and the contribution from non-propagating modes. Experimentally, inelastic neutron scattering has been used to measure phonon lifetimes (MFPs) in materials, but this technique is more suited for single crystal samples.[14] Traditionally, empirical expressions and simple models have been the only means to estimate MFPs in amorphous materials.[15–19]

Predicting the vibrational MFPs requires the group velocity and lifetime of the low-frequency propagating modes.[5–8,10,16,17,20,21] It is typically assumed that the group velocity of the low-frequency modes is equal to the sound speed.[5,8,15–21] The MFPs are then determined by the vibrational lifetimes.

Experimental measurements of the thermal conductivity of thin films of a-SiO_2 and a-Si

at varying temperatures gives indirect information about the low-frequency scaling of the propagating mode lifetimes.[5–8,10,16,17,20–23] However, the scaling of the low-frequency lifetimes has only recently been understood by experimental measurements of a-SiO_2.[10,24–27] For a-Si the low-frequency scaling of the lifetimes is less understood,[5–7,20–23,28] and temperature-varying[22] and film thickness-varying measurements[5–7,20–22,29–35] suggest multiple different scalings. Because of this, the thermal conductivity accumulation function in a-Si is not well understood.[1,5–7,20,21,28]

The objective of this work is to investigate the propagating and non-propagating contributions to thermal conductivity of a-SiO2 and a-Si by predicting the MFPs and thermal conductivity accumulation functions for realistic models. The results are compared with the measurements by Regner et al.[1] and experimental measurements for varying film thicknesses at 300 K.[5–10,16–18,30,36] For the first time, two of the most widely-studied amorphous materials, a-SiO_2 and a-Si, are examined in parallel to understand the experimental results.

The paper is organized as follows. The theoretical formulation and modeling framework is discussed in Section II. Sample preparation for our models of bulk a-SiO_2 and a-Si is discussed in Section III A. Harmonic lattice dynamics calculations are performed on large models and the vibrational density of states is calculated in Section . The plane-wave character of the harmonic vibrational modes is analyzed in Section IV B. By analyzing their plane-wave character, the group velocity of the low-frequency propagating modes is predicted and compared to two alternative predictive methods in Section IV.

Once the group velocity of the propagating modes is specified, the vibrational mode lifetimes are predicted using the molecular dynamics-based normal mode decomposition method in Section IV D. Using the mode group velocities and lifetimes, the vibrational mode diffusivities are predicted and compared with predictions from the Allen-Feldman (AF) theory in Section IV E. Predicting the diffusivities (i.e., the product of the squared group velocity and lifetimes) of the propagating modes allows for a direct comparison with the non-propagating modes, where group velocity and lifetimes are not well-defined.[3] Using this comparison, a cutoff frequency between propagating and non-propagating modes is identified for a-SiO_2 and a-Si.

The properties of the propagating and non-propagating modes are used to predict a bottom-up total thermal conductivity in Section V A. Using the Green-Kubo method and molecular dynamics simulations of very large models of bulk a-SiO_2 and a-Si (including,

to our knowledge, the largest molecular dynamics simulation for a model of a-Si[28,37]), we predict a top-down total thermal conductivity in Section V A. By comparing the bottom-up and top-down thermal conductivity predictions, we verify the scaling of the lifetimes of the propagating modes for our model of bulk a-Si. From the bottom-up approach, the spectrum of vibrational MFPs and the thermal conductivity accumulation functions are predicted for the first time for a-SiO_2 and a-Si in Section V B. The results are compared with the measurements of Regner et al.[1] and experiments on thin films.[5–10,16–18,30,36]

II. THEORETICAL FORMULATION OF VIBRATIONAL THERMAL CONDUCTIVITY

We calculate the total vibrational thermal conductivity, k_{vib}, of an amorphous solid from

$$k_{vib} = k_{pr} + k_{AF}, \tag{1}$$

where k_{pr} is the contribution from propagating modes[38–40] and k_{AF} is the contribution from non-propagating modes predicted by the AF theory.[20] Mode-level properties obtained from molecular dynamics (MD) simulations and lattice dynamics calculations will be used as inputs. Equation (1) has been used in previous studies of amorphous materials,[5–8,10,16,17,20,21] leading to predictions that while k_{pr} is a negligible fraction of k_{vib} for a-SiO_2 ($< 10\%$),[8,10,16,17] it is non-negligible for a-Si ($> 20\%$).[5–7,20,21,28]

The propagating contribution is modeled as[20,21]

$$k_{pr} = \frac{1}{V}\int_0^{\omega_{cut}} DOS(\omega)C(\omega)D_{pr}(\omega)d\omega, \tag{2}$$

where V is the system volume, ω is the mode frequency, ω_{cut} is the maximum frequency of propagating modes, $DOS(\omega)$ is the vibrational density of states (DOS), $C(\omega)$ is the mode specific heat, and $D_{pr}(\omega)$ is the mode diffusivity. When using mode properties obtained from calculations on finite-sized systems, it is common to write Eq. (2) as a summation over the available modes.[20,21] We choose the integral form because the required use of finite-sized simulation cells limit the lowest frequency modes that can be accessed. An extrapolation must be made to the zero frequency limit which is more easily handled with the integral.[5–8,10,20,21] Equation (2) is obtained by using the single-mode relaxation time approximation to solve the Boltzmann transport equation for a phonon gas.[40] In the derivation of Eq. (2), the system

is assumed to be isotropic (valid for an amorphous material) and have a single polarization, making the mode properties only a function of frequency. The choice of a single polarization (i.e., an averaging of the transverse and longitudinal branches) does not significantly change the results predicted in this work or that of others.[5–7,10,20,21] We will evaluate Eq. (2) under the Debye approximation, which assumes isotropic and linear dispersion such that the the DOS is

$$DOS(\omega) = \frac{3\pi\omega^2}{2v_s^3}, \tag{3}$$

where v_s is an appropriate sound speed.[38]

The specific heat in the classical, harmonic limit is k_B, where k_B is the Boltzmann constant.[41] Taking this classical limit allows for a direct comparison between the lattice dynamics-based predictions and those from the classical MD simulations. The harmonic approximation has been found to be valid for systems ranging from Lennard-Jones (LJ) argon[42], to crystalline Stillinger-Weber silicon and carbon nanotubes[43] at temperatures below half the melting temperature. The full quantum expression for the specific heat is[40]

$$C(\omega) = k_\mathrm{B}\left[\frac{\hbar\omega/2k_\mathrm{B}T}{\sinh(\hbar\omega/2k_\mathrm{B}T)}\right]^2, \tag{4}$$

where $\hbar$ is the Planck constant.[38] The quantum specific heat will be used for the high-frequency non-propagating modes to compare the k_{AF} predictions to experimental measurements in Sections V A and V B.

The diffusivity of the propagating modes is

$$D_{pr}(\omega) = \frac{1}{3}v_s^2\tau(\omega), \tag{5}$$

where $\tau(\omega)$ is the frequency-dependent mode lifetime.[40] An equivalent physical picture in terms of a scattering length is

$$D_{pr}(\omega) = \frac{1}{3}v_s\Lambda(\omega), \tag{6}$$

where $\Lambda(\omega)$ is the phonon mean free path (MFP), defined as

$$\Lambda(\omega) = v_s\tau(\omega). \tag{7}$$

The lifetimes will be modeled using

$$\tau(\omega) = B\omega^{-n}. \tag{8}$$

For amorphous materials, the scaling exponent n has been found experimentally and numerically to be between two and four.[6,7,20,21,24–28,44–62] A value of two corresponds to Umklapp scattering,[63] while a value of four corresponds to Rayleigh scattering from point defects.[64] Combined with [Eq. (3)], choosing $n \leq 2$ ensures that the thermal conductivity evaluated from Eq. (2) is finite. Choosing $n > 2$ causes the thermal conductivity to diverge, which can be fixed using additional anharmonic[20,21] or boundary scattering terms.[5–7]

The AF diffuson contribution to thermal conductivity is[20,21]

$$k_{AF} = \frac{1}{V} \sum_{i,\omega_i > \omega_{cut}} C(\omega_i) D_{AF}(\omega_i), \tag{9}$$

where ω_i is the frequency of the ith diffuson mode, $C(\omega_i)$ is the diffuson specific heat, and $D_{AF}(\omega_i)$ is the diffuson diffusivity. Equation (9) is written as a sum because there are enough high-frequency diffusons in the finite-size systems studied here to ensure a converged value.[20,21] The AF diffusivities are calculated from[3]

$$D_{AF}(\omega_i) = \frac{\pi V^2}{\hbar^2 \omega_i^2} \sum_{j \neq i} |S_{ij}|^2 \delta(\omega_i - \omega_j), \tag{10}$$

where δ is the Dirac delta function.[65] The heat current operator S_{ij}, which measures the thermal coupling between vibrational modes i and j based on their frequencies and spatial overlap of eigenvectors, can be calculated from harmonic lattice dynamics theory.[3,20,21] For Eq. (10), S_{ij} is directionally averaged because amorphous materials are isotropic.

III. CALCULATION DETAILS

A. Sample Preparation

The three smallest a-SiO_2 samples are the same as those used in Ref. 66 and contain 288, 576, and 972 atoms at a density of 2350 kg/m^3. These samples were prepared using a melt-quench procedure using the MD package LAMMPS and a time step of 0.905 fs.[67] Larger systems of 2880, 4608, and 34,562 atoms were created by tiling the smaller samples, melting at a temperature of 10,000 K and quenching instantaneously to a temperature of 300 K at constant volume. The resulting a-SiO_2 structure contains a network of rigidly-bonded SiO_4 tetrahedral sub-units, which are weakly bonded via shared oxygen atoms and are shown in Fig. 1 (a). The 34,562 atom sample has a supercell side length of 8.052 nm.

The atomic interactions are modeled using the modified Beest-Kramer-van Santen (BKS) potential[68,69] from Ref. 66, except that the 24-6 LJ potential[70] is changed to a 12-6, which has a negligible effect on the predictions. The LJ potentials use a cutoff of 8.5 $\mathring{A}$ and the Buckingham potentials use a cutoff of 10 $\mathring{A}$. The electrostatic interactions are handled using the Wolf direct summation method with a damping parameter of $0.223\mathring{A}^{-1}$ and a cutoff of 12 $\mathring{A}$.[71]

For a-Si, we use samples with 216, 1000, 4096, and 100,000 atoms generated from the modified Wooten-Winer-Weaire (WWW) algorithm from Ref. 37. The resulting a-Si structure is a predominantly tetrahedrally bonded network[37] and is shown in Fig. 1 (b). A larger sample was created from the 100,000 atom sample by tiling it twice in all directions to create an 800,000 atom sample with a side length of 24.81 nm. All a-Si structures have a density of 2330 kg/m^3, equivalent to the perfect crystal with a lattice constant of 5.43 $\mathring{A}$. The SW potential is used to model the atomic interactions.[72] The MD simulations are performed using LAMMPS with a time step of 0.5 fs.

Amorphous materials may have many different atomic configurations with nearly equivalent potential energies, leading to potential metastability during MD simulations.[21,28,73–75] This meta-stability can cause errors when predicting vibrational lifetimes using normal mode decomposition (NMD, see Section IV D). To remove metastability, all a-SiO_2 and a-Si samples were annealed at a temperature of 1100 K for 10 ns.[21,28] The removal of meta-stability is demonstrated by a decrease and plateau of the sample's potential energy during the annealing.

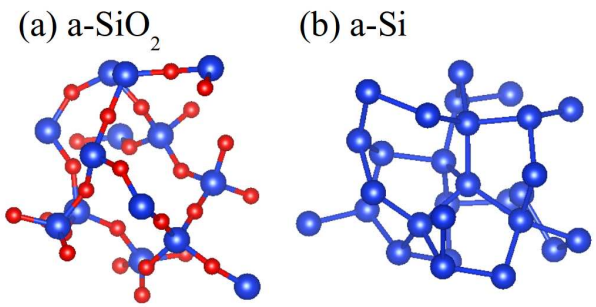

FIG. 1: (a) Small sample of a-SiO_2 created from a melt-quench technique showing the Si-O tetrahedral bond network. Bond lengths range between 1.6 and 1.8 $\mathring{A}$. (b) Small sample structure of a-Si created by the modified WWW algorithm. Bond lengths range between 2.3 and 2.7 $\mathring{A}$. Visualizations using the VESTA package.[76]

B. Simulation Details

Before data collection, all MD simulations are first equilibrated in an NVT (constant number of atoms, volume, and temperature) ensemble for 10^6 time steps at a temperature of 300 K. Data are then collected from simulations in the NVE (constant number of atoms, volume, and total energy) ensemble for 2^{21} time steps where the atomic trajectories are sampled every 2^8 time steps. Ten MD simulations with different initial conditions are run and the predictions are ensemble averaged.

The Green-Kubo (GK) method is used to predict a top-down thermal conductivity k_{GK} [i.e., without using Eq. (1)][41] using the first-avalanche method to specify the converged value of the integral of the heat current autocorrelation function (Section V A.[77] For system sizes of 4,608 (a-SiO_2, supercell side length of 4.026 nm) and 4,096 (a-Si, supercell side length of 4.344 nm) atoms, the trajectories from the MD simulations are also used to predict the vibrational mode lifetimes using the NMD method (Section IV D).

For an amorphous supercell, the only allowed wave vector is the Gamma point (i.e., $\boldsymbol{\kappa} = 0$), where $\boldsymbol{\kappa}$ is the wavevector and there are $3N_a$ polarization branches labeled by ν, where N_a is the number of atoms. Calculation of the vibrational modes at the Gamma point requires the eigenvalue solution of a dynamical matrix of size $(3N_a)^2$ that scales as $[(3N_a)^2]^3$, limiting the system sizes that can be considered to 4,608 (a-SiO_2) and 4,096 (a-Si) atoms. The eigenvalue solution is also required to predict the vibrational DOS (Section IV A) and structure factors (Section IV B), and to perform the NMD calculations (Section IV D) and AF calculations (Section IV E). The frequencies and eigenvectors were computed using harmonic lattice dynamics calculations with GULP.[78] The calculation of the AF thermal diffusivities [Eq. (10)] is performed using GULP and a Lorentzian broadening of $14\delta\omega_{avg}$ for a-SiO_2 and $5\delta\omega_{avg}$ for a-Si, where $\delta\omega_{avg}$ is the average mode frequency spacing [$\delta\omega_{avg} = 1.8 \times 10^{10}$ (a-SiO_2) and 1.0×10^{10} (a-Si) rads/s].[20,21] Varying the broadening by 10 % around these values does not change the resulting thermal conductivity k_{AF} within the uncertainties (see Section V A).

IV. VIBRATIONAL PROPERTIES

A. Density of States

The vibrational DOS is computed from

$$DOS(\omega) = \sum_i \delta(\omega_i - \omega), \tag{11}$$

where a unit step function of width $100\delta\omega_{avg}$ is used to broaden $\delta(\omega_i - \omega)$. The results for a-$SiO_2$ and a-Si are plotted in Fig. 2. The DOS for a-Si is similar to that of crystalline silicon,[4,79] with peaks at mid- and high-frequencies. The DOS for a-SiO_2 is constant over most of the frequency-range, with a gap that separates the high-frequency Si-O interactions.[66] There is a clear ω^{-2} scaling for both a-Si and a-SiO_2 at the lowest frequencies. The onset of this scaling occurs at a higher frequency for a-Si (between 1.5 $\times 10^{13}$ rads/s) than a-SiO_2 (between 4.5 $\times 10^{12}$ rads/s). This low-frequency scaling is predicted by the Debye model [Eq. (3)] and suggests that these modes may be propagating (i.e., phonon-like).

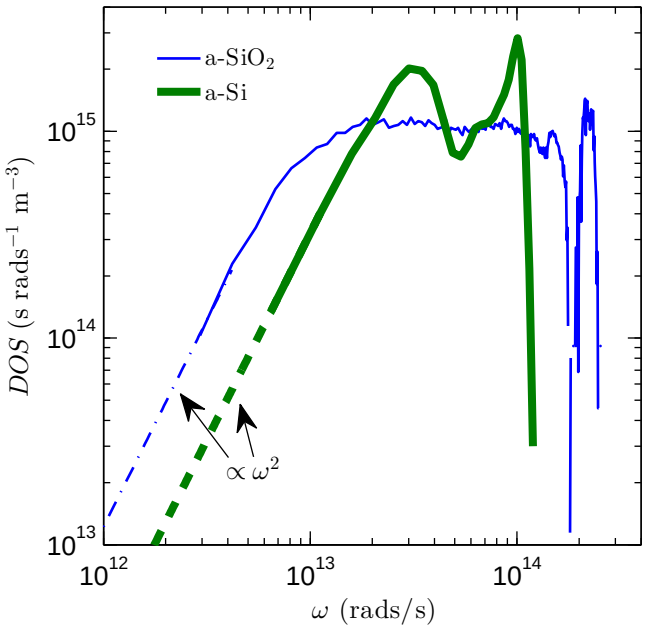

FIG. 2: Vibrational DOS of a-SiO_2 and a-Si plotted on a log-log scale. Both models show an ω^{-2} scaling at low frequency. The DOS for a-Si has two peaks similar to the DOS of the crystalline phase.[80] The DOS for a-SiO_2 is flat over most of the spectrum, with a high frequency gap that separates the Si-O interactions.[66]

B. Structure Factor

Calculating the structure factors of the supercell Gamma modes is a method to test for their propagating (i.e., plane-wave) character at a particular wavevector and polarization. This approach has been previously used to predict effective dispersion curves of disordered and amorphous materials experimentally[10,25,27,45,49,50,81–84] and numerically.[4,20,21,46–48,51,53,56,57,61,85–90] The structure factor at a wavevector $\boldsymbol{\kappa}$ is defined as[4]

$$S^{L,T}(\substack{\boldsymbol{\kappa}\\ \omega}) = \sum_{\nu} E^{L,T}(\substack{\boldsymbol{\kappa}\\ \nu})\, \delta(\omega - \omega(\substack{\boldsymbol{\kappa}=\mathbf{0}\\ \nu})), \tag{12}$$

where the summation is over the Gamma modes, E^T refers to the transverse polarization and is defined as

$$E^{L}(\substack{\boldsymbol{\kappa}\\ \nu}) = \left| \sum_{b} \hat{\boldsymbol{\kappa}} \cdot e(\substack{\boldsymbol{\kappa}=\mathbf{0}\ b\\ \nu\ \ \alpha}) \exp[i\boldsymbol{\kappa} \cdot \boldsymbol{r}_0(\substack{l=0\\ b})] \right|^2 \tag{13}$$

and E^L refers to the longitudinal polarization and is defined as

$$E^{T}(\substack{\boldsymbol{\kappa}\\ \nu}) = \left| \sum_{b} \hat{\boldsymbol{\kappa}} \times e(\substack{\boldsymbol{\kappa}=\mathbf{0}\ b\\ \nu\ \ \alpha}) \exp[i\boldsymbol{\kappa} \cdot \boldsymbol{r}_0(\substack{l=0\\ b})] \right|^2 . \tag{14}$$

In Eqs. (13) and (14), the b summations are over the atoms in the disordered supercell, $\boldsymbol{r}_0(\substack{l=0\\ b})$ refers to the equilibrium atomic position of atom b, l labels the unit cells ($l = 0$ for the supercell), α labels the Cartesian coordinates, and $\hat{\boldsymbol{\kappa}}$ is a unit vector. The vibrational mode shape is contained in the $3N_a$ components of its eigenvector, $e(\substack{\boldsymbol{\kappa}=\mathbf{0}\ b\\ \nu\ \ \alpha})$.[39]

The transverse and longitudinal structure factors are plotted in Figs. 3(a) and 3(b) for a-SiO_2 and a-Si for wavevectors along the [100] direction of the supercells. Because amorphous structures are isotropic, the structure factors are direction-independent. Mode frequencies $[\omega_0(\boldsymbol{\kappa})]$ and linewidths $[\Gamma(\boldsymbol{\kappa})]$ can be predicted by fitting each structure factor peak $S^{L,T}(\substack{\boldsymbol{\kappa}\\ \omega})$ to a Lorentzian function of the form

$$S^{L,T}(\substack{\boldsymbol{\kappa}\\ \omega}) = \frac{C_0(\boldsymbol{\kappa})}{[\omega_0(\boldsymbol{\kappa}) - \omega]^2 + \Gamma^2(\boldsymbol{\kappa})}, \tag{15}$$

where $C_0(\boldsymbol{\kappa})$ is a constant related to the DOS.[88] A dispersion relation is identified by plotting the $\omega_0(\boldsymbol{\kappa})$ values in the middle panels of Figs. 3(a) and 3(b), where the error bars indicate the linewidths. For a-Si, Lorentzian fits to the structure factor peaks have coefficients of determination[91] greater than 0.8 for $|\boldsymbol{\kappa}|/\kappa_{max} \leq 0.75$ and less than 0.7 for $|\boldsymbol{\kappa}|/\kappa_{max} > 0.75$, where $\kappa_{max} = 2\pi/a$ and a is the lattice constant of the crystalline phases of silica (4.8 $\mathring{A}$)

and silicon (5.43 $\mathring{A}$).[66,72] For a-SiO_2, the coefficients of determination are greater than 0.8 for $|\boldsymbol{\kappa}|/\kappa_{max} \leq 0.2$ and less than 0.7 for larger wavevectors, where the structure factors peaks are less than an order of magnitude larger than the background.

For a-Si, the extracted dispersion is nearly linear at small wavevectors with a slight decrease in slope at the largest values.[20,21] For a-SiO_2, the dispersion is concave-down for the smallest wavevectors considered, transitioning to a strong concave-up dispersion at intermediate wavevectors. For the intermediate wavevectors, the longitudinal dispersion for a-SiO_2 is well-described by the so-called "dispersion law for diffusons," where $\omega \propto \kappa^2$.[88] This large concave-up dispersion has been observed in experimental measurements and numerical models of amorphous materials[10,46,51,53,82] including a-SiO_2.[10,46,51,82] We note that at frequencies lower than 6.28×10^{11} rads/s, experimental measurements of a-SiO_2 recover a linear dispersion.[10,25,27,50,82] This frequency range is not accessible with the models studied in this work.

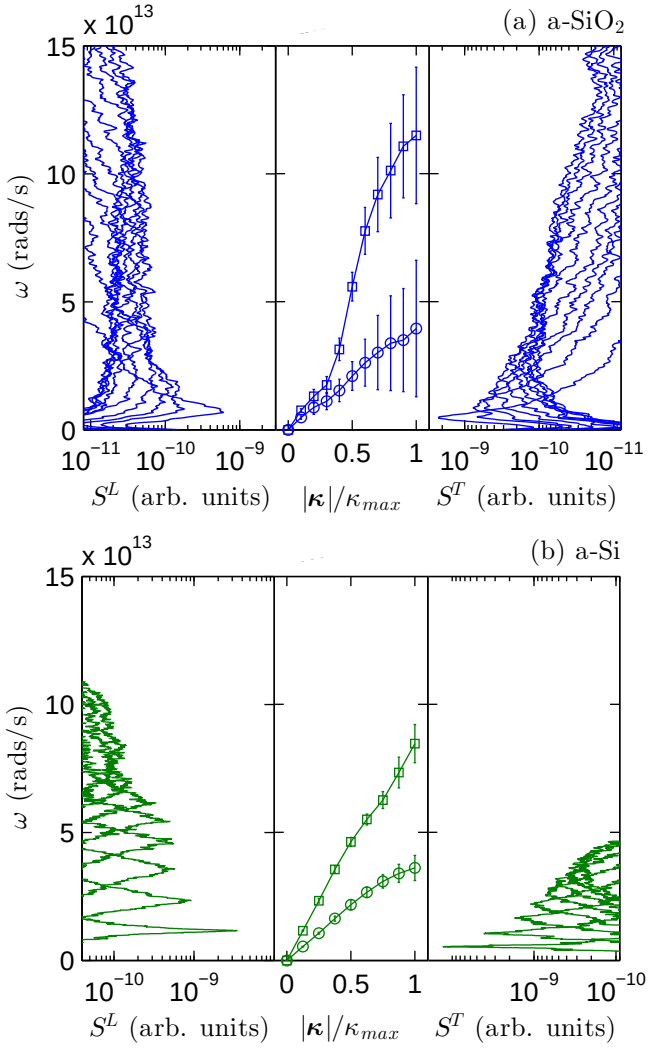

FIG. 3: Longitudinal (left panel) and transverse (right panel) structure factors [Eq. (12)] for (a) a-SiO_2 and (b) a-Si. The wavevectors are normalized by $\kappa_{max} = 2\pi/a$, where a is 4.8(a-SiO_2) and 5.43(a-Si) $\mathring{A}$, based on the lattice constants of the crystalline phases.[66,72]

C. Group Velocity

For a disordered solid, except for the transverse and longitudinal sound speeds, there is not an accepted method to predict the group velocity of individual vibrational modes. While the structure factor gives the frequency spectrum needed to construct a propagating state with pure wavevector $\boldsymbol{\kappa}$, the individual mode spectra $E^T(\overset{\boldsymbol{\kappa}}{\nu})$ and $E^L(\overset{\boldsymbol{\kappa}}{\nu})$ predict the plane-wave character of each mode.[4,92] It is not generally possible to assign a unique wavevector to individual modes, even at low frequency,[4,92] which makes predicting their group velocities challenging. While attempts have been made to predict individual mode group velocities,[28,79,93–96] but there is no theoretical basis for the proposed methods.

We now use the DOS and structure factors predicted in Sections IV A and IV B to predict the group velocities of the low-frequency modes for a-SiO_2 and a-Si. By fitting the DOS from Fig. 2 to Eq. (3), a sound speed is obtained and is reported in Table I. Because the DOS is a mixture of transverse and longitudinal modes, only a single sound speed can be predicted.

Both longitudinal and transverse sound speeds can be predicted from the structure factor peaks by forward differencing the dispersion relation as

$$v_s = \frac{\omega_0(\kappa_{min})}{\kappa_{min}}. \tag{16}$$

The results are provided in Table I. The transverse and longitudinal sound speeds of a material can also be predicted from the material's bulk (G) and shear (K) moduli from

$$v_{s,T} = \frac{G}{\rho}^{1/2} \tag{17}$$

and

$$v_{s,L} = \frac{4G + 3K}{3\rho}^{1/2}. \tag{18}$$

Using the bulk and shear moduli defined in terms of the elastic constants according to the Voight convention,[78] the corresponding sound speeds are reported in Table I.

The longitudinal and transverse sound speeds for a-SiO_2 predicted using the bulk and shear moduli are in reasonable agreement with predictions using a linear fit to the peaks of the current correlation function for a model with 8,016 atoms using the BKS potential [3,568 (transverse) and 5,937 (longitudinal) m/s].[51] Experimental measurements of the sound speeds using Brillouin light and inelastic x-ray scattering range between 3,800-4,000 (transverse) and 6,000-6,400 (longitudinal) m/s.[45,50,82,97,98] Differences between our predictions and

experimental measurements could be attributed to the limitation of the BKS potential for modeling a-SiO_2.

Our predictions for a-Si using all three methods (Table I are within 10% of predictions from the elastic moduli[99,100] and structure factor[53] from previous models created by the original WWW algorithm.[101] The 4096 atom model created by the modified WWW algorithm[37] predicted 7,670 (longitudinal) m/s from the structure factor,[56] within 5% of our prediction. In an attempt to explain the anomalously high longitudinal sound speed (8,300 m/s) and thermal conductivity measurements in Ref. 6, three 1,000 atom models relaxed using a tight-binding electron structure method predicted an average of 4,740 (transverse) and 7,830 (longitudinal) m/s.[6] By annealing our structures (Section III A), the sound speeds predicted by the elastic moduli are increased, but not in the amount reported in Ref. 6. Experimental measurements using Rayleigh wave scattering are 3,420 and 4,290 (transverse) m/s for sputtered thin films and ion-bombarded a-Si,[102] which is within 15% of the predictions from our models.

By comparing the sound speeds in Table I, it is clear that the low-frequency DOS of our models for a-Si and a-SiO_2 are dominated by transverse modes. The smaller values predicted by the structure factors and DOS results from the concave-down dispersion seen at low wavevector, particularly for a-SiO_2. The concave-down dispersion is less pronounced for a-Si, where the sound speeds predicted by all three methods are within five percent. The transverse sound speed predicted for our model of a-SiO_2 is about 85% of that predicted by the other methods used here (Table I) and that measured by experiment.[45,50,82,97,98] While using a smaller transverse sound speed leads to an underprediction of the mode diffusivity scaling [Eq. (5), Fig. 5 (a)], it leads to an overprediction of the DOS [Eq. (3)]. Holding all other input parameters in Eq. (1) constant, a smaller sound speed leads to a larger k_{pr} because the DOS scales as $1/v_s^3$. We can thus regard the prediction for k_{pr} with $v_{s,DOS}$ as an upper bound. The transverse sound speed $v_{s,DOS}$ is used for both a-SiO_2 and a-Si throughout the rest of this work, allowing for the use of a single polarization for the propagating contribution [Eq. (2)].

TABLE I: Longitudinal and transverse sound speed estimated from the elastic moduli [Eqs. (18) and (17)], DOS [Eq. (3)], and structure factors [Eq. (16)]. The pre-annealed group velocities predicted by the elastic constants are $v_{s,T} = 3,670$, $v_{s,L} = 7,840$ m/s for a-Si and $v_{s,T} = 2,541$, $v_{s,L} = 4,761$ m/s for a-SiO_2 (see Section IV B).

method	moduli (m/s)	S^T, S^L (m/s)	DOS (m/s)
a-SiO_2			
transverse	3,161	2,732	2,528
longitudinal	5,100	4,779	
a-Si			
transverse	3,886	3,699	3,615
longitudinal	8,271	8,047	

D. Lifetimes

We now predict the lifetimes of all vibrational modes in our models of a-SiO_2 and a-Si using the MD simulation-based NMD method,[28,42,43,96,103–105] which explicitly includes the disorder in the supercell.[28,89,94,95,106] In NMD, the atomic trajectories from an MD simulation are first mapped onto the vibrational mode coordinate time derivatives,[39]

$$\dot{q}(\substack{\boldsymbol{\kappa}=\mathbf{0}\\ \nu}; t) = \sum_{\alpha,b,l}^{3,n,N} \sqrt{\frac{m_b}{N}} \dot{u}_\alpha(\substack{l\\ b}; t)\, e^*(\substack{\boldsymbol{\kappa}=\mathbf{0}\ b\\ \nu\ \ \alpha}) \exp[i(\mathbf{0} \cdot \mathbf{r}_0(\substack{l\\ 0}))]. \tag{19}$$

Here, m_b is the mass of the b_{th} atom in the supercell, $\dot{u}_\alpha$ is the α-component of the atomic velocity, and t is time. Because the supercells of a-SiO_2 and a-Si are disordered, the NMD method can only be performed at the Gamma point ($\boldsymbol{\kappa} = \mathbf{0}$). The spectral energy of each vibrational mode, $\Phi(\nu, \omega)$, is calculated from

$$\Phi(\nu, \omega) = \lim_{\tau_0 \to \infty} \frac{1}{2\tau_0} \left| \frac{1}{\sqrt{2\pi}} \int_0^{\tau_0} \dot{q}(\substack{\boldsymbol{\kappa}=\mathbf{0}\\ \nu}; t) \exp(-i\omega t) dt \right|^2. \tag{20}$$

We choose the frequency-domain representation of the normal mode energy because we find it to be less sensitive to metastability of the amorphous structure than the time-domain representation.

The vibrational mode frequency and lifetime are predicted by fitting each mode's spectral

energy to a Lorentzian function,

$$\Phi(\nu,\omega) = \frac{C_0(\nu)}{[\omega_0(\nu)-\omega]^2+\Gamma^2(\nu)}, \tag{21}$$

where the constant $C_0(\nu)$ is related to the average energy of each mode. This expression is valid when the linewidth $\Gamma(\nu) << \omega_0(\nu)$.[43] The mode lifetime is[103,105]

$$\tau(\nu) = \frac{1}{2\Gamma(\nu)}. \tag{22}$$

The NMD-predicted lifetimes are plotted in Figs. 4 (a) and 4 (b) for a-SiO_2 and a-Si. Also plotted are the timescales extracted from the structure factor linewidths, $1/[2\Gamma(\kappa)]$ (Section IV B). For a-SiO_2, the NMD lifetimes are larger than the Ioffe-Regel (IR) limit $\tau = 2\pi/\omega$,[46] and are bounded by this limit at low frequencies. There is no clear evidence for an ω^{-2} scaling, which would correspond to propagating modes. At mid-frequencies, the NMD lifetimes are approximately constant and there is a peak near 2 $\times 10^{14}$ rads/s, which corresponds to the peak in the DOS (see Fig. 2). The lifetimes predicted from the structure factor fall below the NMD-predicted lifetimes and the IR limit. These low values result because the structure factor for a-SiO_2 is evaluated for large wavevectors where the resulting wavepackets are formed by non-propagating modes.[4,20,21]

For a-Si, the NMD lifetimes show a clear ω^{-2} scaling at low frequency. The lifetimes plateau at higher frequencies, over a wider range of frequencies than for a-SiO_2, with two peaks corresponding to the peaks in the DOS (Fig. 2). A similar plateau of lifetimes at high frequencies has been reported for disordered lattices[89,106,107] and other models of a-Si.[28] The transition from the low-frequency scaling to the plateau region occurs near 10^{13} rads/s, which corresponds to where the DOS first peaks in Fig. 2. Similar behavior has been observed for models of disordered lattices.[89] The lifetimes predicted by the structure factor are in good agreement with those predicted by NMD at low frequencies. Similar agreement has been reported in other models of amorphous materials.[21,108–110] The agreement between the NMD-predicted lifetimes and the structure factor timescales for a-Si at low frequencies indicates that these modes are plane-wave like and the wavepackets formed by these modes are propagating.[4,20,21]

The NMD-predicted lifetimes for a-Si range from 0.5 to 10 ps and are similar in magnitude to those predicted for previous models of a-Si.[109–112] We note that one previous study of a-Si modeled using the Tersoff potential predicted vibrational lifetimes on the order of 100 ps,

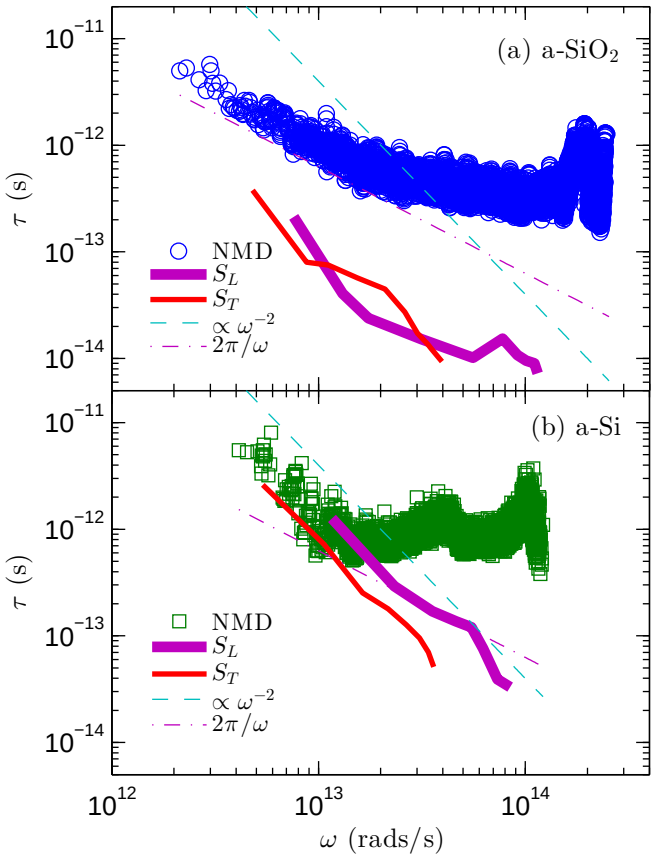

FIG. 4: Vibrational mode lifetimes predicted by NMD [Eq. (22)] and the structure factors [Eq. (15)] for (a) a-SiO_2 and (b) a-Si. The NMD-predicted lifetimes are larger than the IR limit while the lifetimes predicted from the structure factors fall below the IR limit, particularly for a-SiO_2. The NMD-predicted lifetimes show a plateau at high-frequencies. For a-Si, a clear ω^{-2} scaling is observed at low frequencies, while the lifetimes plateau at higher frequencies, over a wider range of frequencies than for a-SiO_2, with two peaks corresponding to the peaks in the DOS (Fig. 2). The transition from the low-frequency scaling to the plateau region occurs near 10^{13} rads/s, which corresponds to where the DOS first peaks in Fig. 2.

an order of magnitude larger than the values reported here and in previous studies.[109–112] It is unclear what the source of this discrepancy is, although in Ref. 28 the NMD analysis was performed in the time domain, where metastability can be more strongly pronounced. Using the Tersoff potential on the WWW a-Si models in this work, we predict similar lifetimes to those from the SW potential.

E. Diffusivities

Using the sound speeds predicted from the DOS (Table I), the NMD-predicted lifetimes for a-SiO_2 and a-Si are used to predict the mode diffusivities with Eq. (5). The results are plotted in Figs. 5 (a) and 5 (b). We note that the sound speed is most appropriate for the lowest-frequency modes, where the DOS scales as ω^2 (Fig. 2). The AF theory is also used to predict the mode diffusivities, and the results are also plotted in Figs. 5 (a) and 5 (b).

For a-SiO_2, the mode diffusivities predicted by NMD and AF agree well over the majority of the frequency range. The AF diffusivities at the highest frequencies show a sharp decrease, which is an indication that these modes are localized.[20] The low- and mid-frequency diffusivities and are above the high-scatter limit,

$$D_{HS} = \frac{1}{3} v_s a, \tag{23}$$

which assumes that all vibrational modes travel with the sound speed and scatter over a distance of the lattice constant.[18] We use the lattice constant of the crystalline phase (see Section IV B). The low-frequency NMD diffusivities do not show a definitive scaling. Based on the results in Ref. 10, we choose a propagating/non-propagating cutoff frequency of 4.55×10^{12}. The constant B in Eq. (8) for $n = 2$ is then fit to the AF-predicted diffusivities for frequencies below the cutoff by dividing the diffusivities by v_{DOS}. The fit value is $B = 2.95 \times 10^{13}$ s^{-2} This choice is discussed in Section V A.

For a-Si, the mode diffusivities predicted by NMD at low frequencies show a clear ω^{-2} scaling. The NMD-predicted diffusivities are larger and show less scatter than those predicted by the AF theory, which is due to the finite-size system and the broadening that is required to evaluate Eq. (10).[20] By using a larger broadening ($100\delta\omega_{avg}$), the scatter in the AF-predicted diffusivities at low frequency can be smoothed, but at the cost of decreasing the diffusivities at intermediate and high frequencies, which affects the predicted diffuson contribution to thermal conductivity (see Section V A). It is possible that a frequency-dependent broadening may be necessary for a-Si and the AF theory, but determining this dependence is not necessary for interpreting our results. For a-Si the NMD- and AF-predicted diffusivities diverge near a frequency of 10^{13} rads/s. The NMD-predicted diffusivities are relatively constant above this frequency, indicating that the sound speed is no longer an applicable scaling. The AF diffusivities are larger than the high-scatter limit [Eq. (23)], except for the highest frequencies, which are localized.[20]

For a-Si, we choose ω_{cut} and B so that Eq. (5) is equal to the average AF-predicted diffusivity at the cutoff frequency. The resulting values are $\omega_{cut} = 1.16 \times 10^{13}$ rads/s and $B = 2.76 \times 10^{14}$ s^{-2}. This choice allows Eq. (5) to pass reasonably well through both the AF- and NMD-predicted diffusivities.

While experiments show there is a cross-over region for the low-frequency lifetime scaling of ω^{-2} to ω^{-4} for a-SiO_2,[24,27] the region is observed for the frequency range of 4.6×10^9 to 1.52×10^{10} rads/s[24] and 3.04×10^{11} to 1.52×10^{12} rads/s[27]. Experiments are limited for a-Si thin films,[23] and our present models are not large enough to investigate the mode-by-mode properties in this cross-over region. For a-Si, we consider a separate ω^{-4} scaling for Eq. (8) that is discussed in Section V A. Because this scaling is not clear from the data in Fig. 5 (b), we use a cutoff frequency of 1.52 $\times 10^{13}$ rads/s based on Refs. 20 and 5 and choose $B = 2.07 \times 10^{40}$ s^{-4} so that Eq. (5) is equal to the average AF-predicted diffusivity at the cutoff frequency.

Both a-SiO_2 and a-Si have a region at higher frequencies where the AF-predicted mode diffusivities are relatively constant. This behavior has been reported for model disordered systems such as disordered lattices[88,89,107] and jammed systems.[58,60] While diffusons are non-propagating modes whose MFPs are not well-defined,[20] a diffuson MFP can be defined as

$$\Lambda_{AF}(\omega_i) = [3D_{AF}(\omega_i)\tau(\omega_i)]^{1/2}, \tag{24}$$

where $\tau(\omega_i)$ is the NMD-predicted lifetime for that mode. Using this definition, $\Lambda_{AF}(\omega_i)$ for both a-SiO_2 and a-Si is found to vary between the crystalline lattice constant (see Section IV B) and the supercell size (see Section III A) for modes with frequency above the cutoff. Similar MFPs have been estimated for diffusons in a-Si in previous studies.[20,21] For modes with frequency below the cutoff, the NMD-predicted MFPs from Eq. (7) range up to 16 (a-SiO_2) and 43 (a-Si) nm. This result is in contrast to the MFPs estimated in Ref. 28 for a-Si, which ranged up to 500 nm. We believe that the origin of the large MFPs in Ref. 28 is a combination of the predicted lifetimes (see Section IV D) and the method used to estimate the mode group velocities.

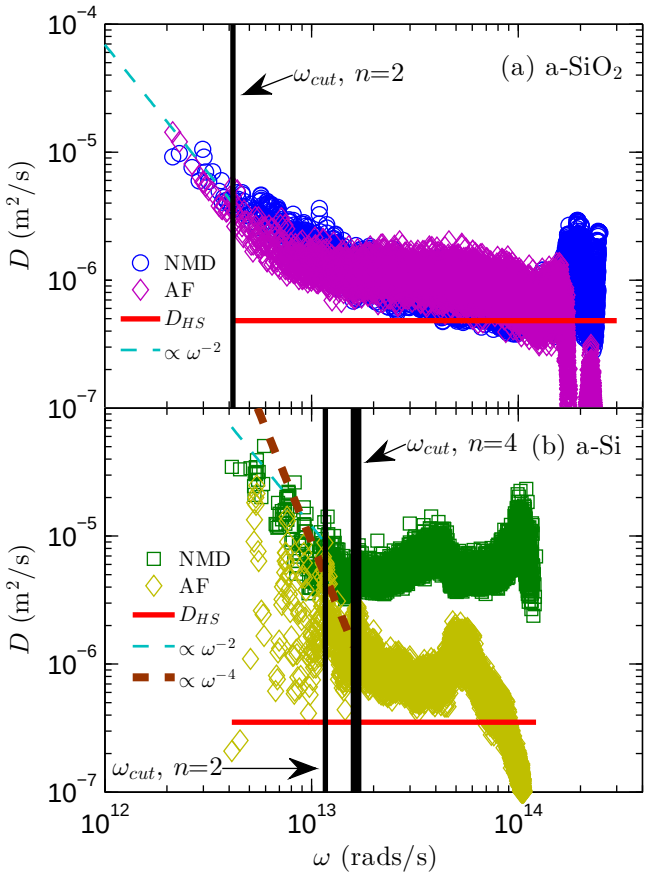

FIG. 5: Vibrational mode diffusivities predicted from NMD [using Eqs. (5) and (22) with the DOS sound speed from Table I] and the AF theory [Eq. (10)]. Also shown are extrapolations based on an ω^{-2} scaling with Eqs. (8) and (5) for a-SiO_2, and an additional ω^{-4} for a-Si. For both systems, the diffusivities are larger than the high-scatter limit [Eq. (23)] except at high frequencies, where the modes are localized.

V. THERMAL CONDUCTIVITY

A. Bulk

To predict the bulk thermal conductivity for our models of a-SiO_2 and a-Si, we use both Eq. (1) and the GK method. The GK method is computationally inexpensive compared to the NMD and AF methods so that larger system sizes can be accessed. The GK-predicted thermal conductivities for a-SiO_2 and a-Si are plotted in Fig. 6 versus the inverse of the system size. For a-SiO_2, there is no system-size dependence. The bulk thermal conductivity is estimated to be 2.1 ± 0.2 W/m-K by averaging over all the samples. This prediction is in agreement with the GK predictions in Ref. 66 within the uncertainties, but larger than the MD-based direct-method predictions in Ref. 113. Shenogin et al. predicted the total thermal conductivity of a-SiO_2 using non-equilibrium MD simulations of the same small structures used in this work, finding 2.0 W/m-K for their largest system which was based on a 972 atom model tiled in one direction six times.[114] Our GK-predicted value is larger than experimental measurements, which range between 1.3 and 1.5 W/m-K,[1,9,18,36] because of the classical nature of the MD simulation and the suitability of the BKS interatomic potential for modeling thermal transport in a-SiO_2.[66,113] Quantum statistical effects are considered later in this section.

For a-Si, there is a clear system-size dependence. Because the low-frequency DOS has the form of Eq. (3) and the diffusivities scale as ω^{-2}, the thermal conductivity will scale as the inverse of the system size. The bulk value can be found by extrapolating to an infinite system size.[43,115,116] The extrapolation is performed using the three largest system sizes,[117] leading to a bulk value of 2.0 ± 0.2 W/m-K, where the uncertainty is estimated from the ensemble averaging for each system size. While it is difficult to create bulk a-Si experimentally,[102] our extrapolated bulk value is in reasonable agreement with experimental values for a wide range of thin film thicknesses (see Fig. 7).

To predict thermal conductivity from Eq. (1), we use the parameters B and ω_{cut} specified in Section IV E assuming an ω^{-2} scaling below ω_{cut} and the AF-predicted diffusivities. For a-SiO_2, the propagating, non-propagating, and total thermal conductivities are 0.10 ± 0.05, 1.9 ± 0.1, and 2.0 ± 0.1 W/m-K (see Table II). The uncertainties are estimated by varying ω_{cut} and the AF broadening by 10%. The total value agrees with the GK value within the

uncertainties. For the propagating contribution using an expression similar to Eq. (2), Baldi et al. estimated 0.1 W/m-K[10] and Love and Anderson estimated 0.03 W/m-K.[8]

By using the ω^{-2} diffusivity scaling for a-Si, the propagating, non-propagating, and total thermal conductivity are 0.6 ± 0.2, 1.2 ± 0.2, and 1.8 ± 0.2 W/m-K. This value for total thermal conductivity is in agreement with the GK-predicted bulk value within the uncertainties. Earlier studies using similar models of a-Si find that k_{pr} is less than half of k_{vib},[20,21] in agreement with our results. A recent study of a-Si modeled using the Tersoff potential found $k_{pr} \approx k_{AF}$.[28] Estimates based on experimental measurements have shown k_{pr} to be as low as 20%[5,21] and as high as 80% of k_{vib}.[6,7]

If an ω^{-4} lifetime scaling is assumed, the thermal conductivity diverges at low frequency. We bound the thermal conductivity by assuming the sample to be a thin film of thickness t_f and modify the lifetimes using the Matthiessen rule,[118]

$$\frac{1}{\tau_{eff}} = \frac{1}{\tau_{bulk}} + \frac{2v_s}{t_f}. \tag{25}$$

Using the largest film thickness from the experimental literature(80 μm)[6] gives a propagating contribution to thermal conductivity of 3.0 ± 0.4 W/m-K. Using the ω^{-2} scaling and this film thickness gives a propagating contribution of 0.6 W/m-K (i.e., there is no effect). While predictions for k_{pr} for a-Si vary based on the assumed scaling of the low-frequency vibrational diffusivities[5–7,20,21,28] all evidence supports that k_{pr} is a significant fraction of the total thermal conductivity.[1,5–7,20,21,28]

In Section II we approximated the specific heat of the propagating and non-propagating modes by the classical, harmonic-limit value of k_B. At a temperature of 300 K, the quantum heat capacity [Eq. (4)] at the largest cutoff frequency for either a-SiO_2 or a-Si is $0.98k_B$, justifying the use of the classical specific heat in the propagating term in Eq. (2). For the AF contribution, however, the effect of quantum specific heat is important. At the highest frequencies in a-SiO_2 and a-Si, the specific heat is $0.073k_B$ and $0.47k_B$. Using Eq. (4) in Eq. (9) gives AF thermal conductivities of 1.4 ± 0.1 and 1.0 ± 0.1 W/m-K for a-SiO_2 and a-Si (Table II). This correction brings the estimate of k_{vib} for a-SiO_2 into good agreement with experimental measurements.[1,9,18,36] For a-Si, the modified k_{AF} is within 20% of the classical-limit value, and does not significantly change the predicted k_{vib}.

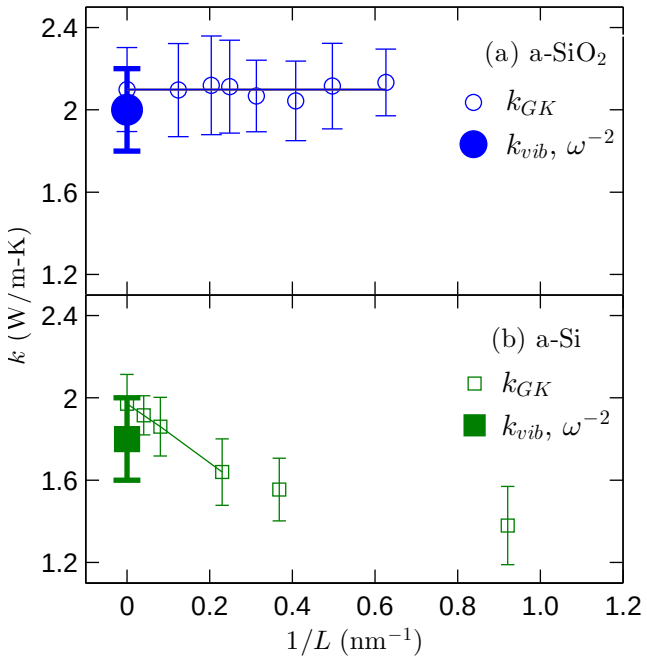

FIG. 6: Thermal conductivities of a-SiO_2 and a-Si predicted using the GK method and Eq. (1). For a-SiO_2, the GK-predicted thermal conductivity is size-independent, indicating that there is no important contribution from propagating modes. For a-Si, there is a clear size dependance, indicating the importance of propagating modes.

TABLE II: Total thermal conductivities for bulk a-SiO_2 and a-Si predicted by the GK method (k_{GK}) and Eq. (1) (k_{vib}). The total thermal conductivity k_{vib} is predicted from the sum of the propagating [k_{pr}, Eq. (2)] and non-propagating [k_{AF}, Eq. (9)] contributions. For the non-propagating contribution, classical and quantum specific heats are considered.

Conductivity (W/m-K)	a-SiO_2	a-Si
k_{GK}	2.1 ± 0.2	2.0 ± 0.2
k_{vib} (classical)	2.0 ± 0.1	1.8 ± 0.2
k_{pr}	0.10 ± 0.05	0.6 ± 0.2
k_{AF} (classical)	1.9 ± 0.1	1.2 ± 0.1
k_{AF} (quantum)	1.4 ± 0.1	1.0 ± 0.1
k_{vib} (quantum)	1.5 ± 0.1	1.6 ± 0.2

B. Accumulation Function

In their broadband frequency domain thermal-reflectance measurements, Regner et al.,[1] following the suggestion of Koh and Cahill,[119] interpret the measured thermal conductivity at a given penetration depth to be representative of the so-called thermal conductivity accumulation function.[11,13] Their results are plotted in Fig. 7 (a) for a 1000 nm thick film of a-SiO_2 and in Fig. 7 (b) for 500 nm and 2000 nm thick films of a-Si. Also plotted in Figs. 7 (a) and 7 (b) are experimental measurements of thin film thermal conductivities. For a-Si, the experimental measurements are grouped broadly by sample preparation technique: (A) chemical vapor deposition[6,7,34] and (B) sputtered.[5,32,33]

Based on the results in Section IV E, we build thermal conductivity accumulation functions for a-SiO_2 and a-Si from

$$k(\Lambda^*) = k_{AF} + \frac{1}{V}\int_{\Lambda_{cut}}^{\Lambda^*} k(\Lambda) d\Lambda, \tag{26}$$

where Λ_{cut} is the MFP at the cut-off frequency, Λ_{max} is the maximum MFP considered in the thermal conductivity accumulation, $k(\Lambda)$ is the thermal conductivity as a function of MFP, and the propagating mode MFPs are calculated using Eq. (7). The non-propagating contribution k_{AF} is evaluated using the quantum specific heat for a-SiO_2 (see Section V A).

The results are plotted in Fig. 7 (a) using $t_f = 1$ μm and in Fig. 7 (b) using $t_f = 80$ μm. While plotting t_f and Λ^* together is an approximate comparison, the thermal conductivity accumulation for varying t_f follows closely the accumulation for an infinite film thickness.

The predicted thermal conductivity accumulation function for a-SiO_2 saturates at a MFP of 10 nm, which is on the order of the finite size of our model. This result is in accord with the penetration depth-independent thermal conductivity measurements using broadband FDTR[1] and experimental measurements that show no film thickness dependance.[9,36]

For a-Si, the low-MFP plateau of thermal conductivity in the measurements of Regner et al. is consistent with our predicted k_{AF}. The propagating contribution to the accumulation is predicted using both ω^{-2} and ω^{-4} lifetime scalings. As discussed in Section V, the ω^{-2} scaling best describes the propagating contribution for our model of bulk a-Si. The thermal conductivity accumulation for the ω^{-2} scaling passes through the largest penetration depth measurements of Regner et al., as well as some of the experimental measurements for varying film thicknesses.

We also consider the ω^{-4} scaling with the boundary scattering model [Eq. (25)]. The measurements of Regner et al. show much sharper accumulations than either the ω^{-2} or ω^{-4} scalings, particularly for a film of thickness 2 μm. Predictions for both the ω^{-2} and ω^{-4} scalings pass reasonably through the experimental measurements. Thermal conductivities as high as 6 W/m-K (not plotted in Fig. 7 (b) have been measured for a-Si thin films deposited using hot-wire chemical vapor deposition (HWCVD). Based on time domain thermal reflectance measurements, the frequency dependence of thermal conductivity of these HWCVD a-Si thin films was found to be similar to SiGe alloys, which suggests an ω^{-4} scaling of the lifetimes of propagating modes. However, our model of bulk a-Si is best described by an ω^{-2} scaling. It is worth noting again that the results from thin film experiments have been interpreted using both ω^{-2} and ω^{-4} scalings.[5–7,20–22]

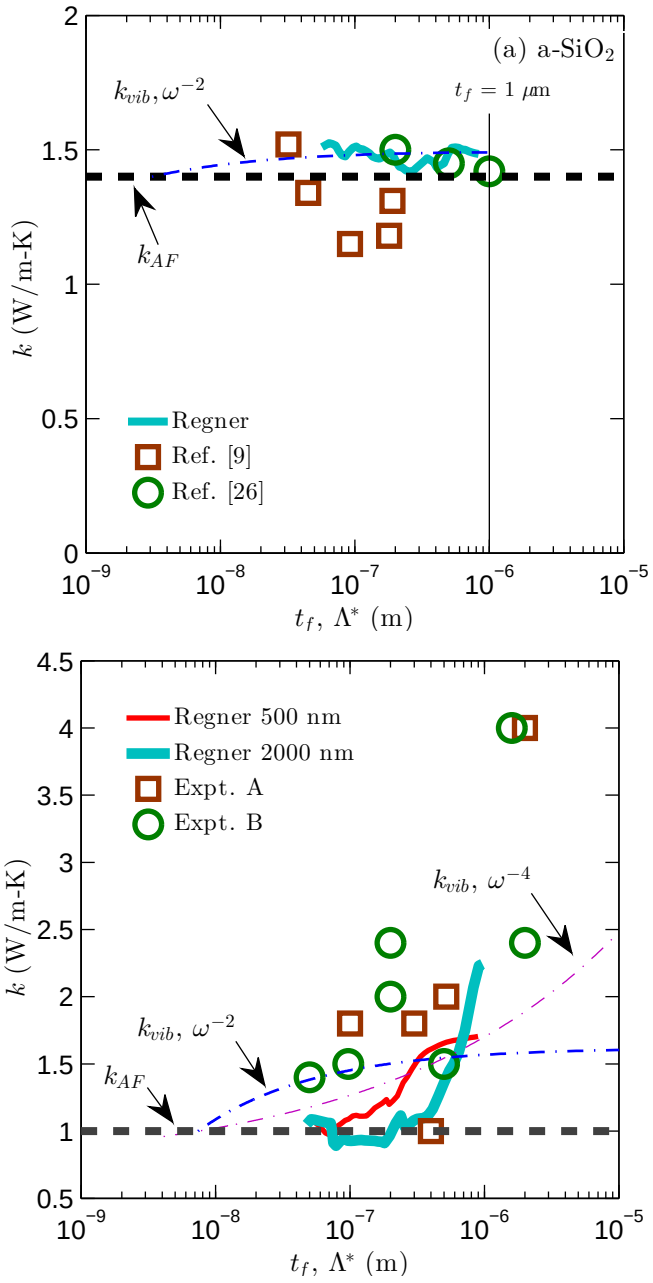

FIG. 7: (a) Predicted thermal conductivity accumulation function [Eq. (26)] for a-SiO_2 compared with experimental broadband frequency domain reflectance measurements by Regner et al.[1] and thin film measurements from Refs. 36 and 9 The predicted thermal conductivity accumulation demonstrates that the propagating contribution is negligible in our model, which is in accord with the experimental measurements. (b) Predicted thermal conductivity accumulation function for a-Si compared with experimental measurements by Regner et al. and thin film measurements using sputtered (Expt. A),[5,32,33] and chemical vapor deposited (Expt. B)[6,7,31,34] deposition techniques for a wide-range of film thicknesses. The predicted thermal conductivity accumulation demonstrates that the propagating contribution is significant for a-Si.

VI. SUMMARY

We investigated the contributions of propagating (k_{ph}) and non-propagating (k_{AF}) modes to the total vibrational thermal conductivity k_{vib} of two amorphous materials, a-SiO_2 and a-Si, using the NMD method (Section IV D), AF theory (Section IV E), and the GK method (Section V A). In accord with experimental results, we find that our model of a-SiO_2 has negligible contribution from propagating modes to total thermal conductivity, while our model of a-Si has non-negligible contribution. The atomic structures of a-SiO_2 and a-Si play an important role in determining the mode-by-mode properties which describe the propagating and non-propagating contributions. The onset of the propagating regime occurs at a higher frequency for a-Si, which is evident from the scaling of the low-frequency DOS and the effective dispersion extracted from the structure factors. This is due, in part, to the weak bonding which exists between individual SiO_4 tetrahedra in a-SiO_2.(cite)

For our model of a-SiO_2, the contribution from propagating modes was shown to be negligible (Section V A). Our predictions align with experimental measurements of the film thickness independence of thermal conductivity[9,36] and penetration depth independence of measurements by Regner et al.[1] While the finite size of our model makes it difficult to identify a clear scaling of the low-frequency lifetime scaling, experiments show that both ω^{-2} and ω^{-4} scalings exist in a-SiO_2,[24,25,27] while the propagating contribution is still negligible.[8–10,36]

For our model of bulk a-Si, the thermal conductivity has significant contribution from propagating modes that are best described by a lifetime scaling of ω^{-2}. Our predicted thermal conductivity accumulation functions are in reasonable agreement with the measurements of Regner et al., while our bulk and thin-film thermal conductivity predictions agree with only a subset of the widely-varying experimental measurements.

The large discrepancies between measurements on a-Si thin films suggest that a comprehensive experimental study using the recently developed broadband techniques[1,12,119] on varying film thicknesses and preparation techniques is necessary. It may be particularly helpful to perform the experiments at temperatures less than 10 K, where the propagating contribution dominates for both a-SiO_2 and a-Si and the low-frequency lifetime scaling is still under debate.[5–8,10,17,18,20,21,30] The thermal conductivity accumulation functions predicted for a-Si using both ω^{-2} and ω^{-4} scalings show reasonable agreement with the experimental measurements from Regner et al.[1] and on thin films.[5–7,20,21] In fact, the existence of ω^{-2} and/or

ω^{-4} scalings has been argued on the basis of the low-temperature (< 10 K) thermal conductivity plateau,[17,20,21] which is observable in some preparations of a-SiO_2[15,17–19] and a-Si[6,29], but absent in others.[6,22,35]

Acknowledgments

This work was supported by AFOSR award FA95501010098 and by a grant of computer time from the DOD High Performance Computing Modernization Program at the US Army Engineer Research and Development Center. We thank Davide Donadio, Joseph Feldman, Asad Hasan, Jonathan Malen, Craig Maloney, Normand Mousseau, Keith Regner, and Michael Widom for helpful discussions.

---

[1] K. T. Regner, D. P. Sellan, Z. Su, C. H. Amon, A. J. McGaughey, and J. A. Malen, Nat Commun **4**, 1640 (2013), URL `http://dx.doi.org/10.1038/ncomms2630`.

[2] R. Sultan, A. D. Avery, J. M. Underwood, S. J. Mason, D. Bassett, and B. L. Zink, Phys. Rev. B **87**, 214305 (2013), URL `http://link.aps.org/doi/10.1103/PhysRevB.87.214305`.

[3] P. B. Allen and J. L. Feldman, Physical Review B **48**, 1258112588 (1993).

[4] P. B. Allen, J. L. Feldman, J. Fabian, and F. Wooten, Philosophical Magazine B **79**, 17151731 (1999).

[5] D. G. Cahill, M. Katiyar, and J. R. Abelson, Physical Review B **50**, 60776081 (1994).

[6] X. Liu, J. L. Feldman, D. G. Cahill, R. S. Crandall, N. Bernstein, D. M. Photiadis, M. J. Mehl, and D. A. Papaconstantopoulos, Phys. Rev. Lett. **102**, 035901 (2009), URL `http://link.aps.org/doi/10.1103/PhysRevLett.102.035901`.

[7] H.-S. Yang, D. G. Cahill, X. Liu, J. L. Feldman, R. S. Crandall, B. A. Sperling, and J. R. Abelson, Phys. Rev. B **81**, 104203 (2010), URL `http://link.aps.org/doi/10.1103/PhysRevB.81.104203`.

[8] M. S. Love and A. C. Anderson, Phys. Rev. B **42**, 18451847 (1990), URL `http://link.aps.org/doi/10.1103/PhysRevB.42.1845`.

[9] S.-M. Lee and D. G. Cahill, Journal of Applied Physics **81**, 25902595 (1997).

[10] G. Baldi, V. M. Giordano, G. Monaco, F. Sette, E. Fabiani, A. Fontana, and G. Ruocco, Phys. Rev. B **77**, 214309 (2008), URL http://link.aps.org/doi/10.1103/PhysRevB.77.214309.

[11] C. Dames and G. Chen, in *Thermoelectrics Handbook: Macro to Nano*, edited by D. M. Rowe (Taylor & Francis, 2005), pp. 421 42–11.

[12] A. J. Minnich, J. A. Johnson, A. J. Schmidt, K. Esfarjani, M. S. Dresselhaus, K. A. Nelson, and G. Chen, Phys. Rev. Lett. **107**, 095901 (2011), URL http://link.aps.org/doi/10.1103/PhysRevLett.107.095901.

[13] F. Yang and C. Dames, Physical Review B **87**, 035437 (2013), URL http://link.aps.org/doi/10.1103/PhysRevB.87.035437.

[14] A. D. Christianson, M. D. Lumsden, O. Delaire, M. B. Stone, D. L. Abernathy, M. A. McGuire, A. S. Sefat, R. Jin, B. C. Sales, D. Mandrus, et al., Phys. Rev. Lett. **101**, 157004 (2008), URL http://link.aps.org/doi/10.1103/PhysRevLett.101.157004.

[15] R. C. Zeller and R. O. Pohl, Phys. Rev. B **4**, 20292041 (1971), URL http://link.aps.org/doi/10.1103/PhysRevB.4.2029.

[16] J. E. Graebner, B. Golding, and L. C. Allen, Phys. Rev. B **34**, 56965701 (1986), URL http://link.aps.org/doi/10.1103/PhysRevB.34.5696.

[17] J. J. Freeman and A. C. Anderson, Phys. Rev. B **34**, 56845690 (1986), URL http://link.aps.org/doi/10.1103/PhysRevB.34.5684.

[18] D. Cahill and R. Pohl, Annual Review of Physical Chemistry **39**, 93121 (1988).

[19] D. G. Cahill and R. O. Pohl, Solid State Communications **70**, 927 930 (1989), ISSN 0038-1098, URL http://www.sciencedirect.com/science/article/pii/0038109889906303.

[20] J. L. Feldman, M. D. Kluge, P. B. Allen, and F. Wooten, Physical Review B **48**, 1258912602 (1993).

[21] J. L. Feldman, P. B. Allen, and S. R. Bickham, Phys. Rev. B **59**, 35513559 (1999), URL http://link.aps.org/doi/10.1103/PhysRevB.59.3551.

[22] B. L. Zink, R. Pietri, and F. Hellman, Physical Review Letters **96**, 055902 (2006), URL http://link.aps.org/doi/10.1103/PhysRevLett.96.055902.

[23] D. B. Hondongwa, B. C. Daly, T. B. Norris, B. Yan, J. Yang, and S. Guha, Phys. Rev. B **83**, 121303 (2011), URL http://link.aps.org/doi/10.1103/PhysRevB.83.121303.

[24] C. Masciovecchio, G. Baldi, S. Caponi, L. Comez, S. Di Fonzo, D. Fioretto, A. Fontana, A. Gessini, S. C. Santucci, F. Sette, et al., Phys. Rev. Lett. **97**, 035501 (2006), URL http:

//link.aps.org/doi/10.1103/PhysRevLett.97.035501.

[25] G. Baldi, V. M. Giordano, G. Monaco, and B. Ruta, Phys. Rev. Lett. **104**, 195501 (2010), URL http://link.aps.org/doi/10.1103/PhysRevLett.104.195501.

[26] G. Baldi, V. M. Giordano, and G. Monaco, Phys. Rev. B **83**, 174203 (2011), URL http://link.aps.org/doi/10.1103/PhysRevB.83.174203.

[27] G. Baldi, M. Zanatta, E. Gilioli, V. Milman, K. Refson, B. Wehinger, B. Winkler, A. Fontana, and G. Monaco, Phys. Rev. Lett. **110**, 185503 (2013), URL http://link.aps.org/doi/10.1103/PhysRevLett.110.185503.

[28] Y. He, D. Donadio, and G. Galli, Applied Physics Letters **98**, 144101 (2011), URL http://link.aip.org/link/?APL/98/144101/1.

[29] G. Pompe and E. Hegenbarth, physica status solidi (b) **147**, 103 (1988), ISSN 1521-3951, URL http://dx.doi.org/10.1002/pssb.2221470109.

[30] D. G. Cahill, H. E. Fischer, T. Klitsner, E. T. Swartz, and R. O. Pohl, Journal of Vaccuum Science and Technology A **7**, 12591266 (1989).

[31] L. Wieczorek, H. Goldsmid, and G. Paul, in *Thermal Conductivity 20*, edited by D. Hasselman and J. Thomas, J.R. (Springer US, 1989), pp. 235–241, ISBN 978-1-4612-8069-9, URL http://dx.doi.org/10.1007/978-1-4613-0761-7_22.

[32] B. S. W. Kuo, J. C. M. Li, and A. W. Schmid, Applied Physics A: Materials Science & Processing **55**, 289296 (1992), ISSN 0947-8396, 10.1007/BF00348399, URL http://dx.doi.org/10.1007/BF00348399.

[33] H. Wada and T. Kamijoh, Japanese Journal of Applied Physics **35**, L648L650 (1996), URL http://jjap.jsap.jp/link?JJAP/35/L648/.

[34] S. Moon, M. Hatano, M. Lee, and C. P. Grigoropoulos, International Journal of Heat and Mass Transfer **45**, 2439 2447 (2002), ISSN 0017-9310, URL http://www.sciencedirect.com/science/article/pii/S0017931001003477.

[35] B. L. Zink, R. Islam, D. J. Smith, and F. Hellman, Phys. Rev. B **74**, 205209 (2006), URL http://link.aps.org/doi/10.1103/PhysRevB.74.205209.

[36] T. Yamane, N. Nagai, S.-i. Katayama, and M. Todoki, Journal of Applied Physics **91**, 97729776 (2002), URL http://link.aip.org/link/?JAP/91/9772/1.

[37] G. T. Barkema and N. Mousseau, Phys. Rev. B **62**, 49854990 (2000), URL http://link.aps.org/doi/10.1103/PhysRevB.62.4985.

[38] N. W. Ashcroft and N. D. Mermin, *Solid State Physics* (Saunders, Fort Worth, 1976).

[39] M. T. Dove, *Introduction to Lattice Dynamics* (Cambridge, Cambridge, 1993).

[40] J. M. Ziman, *Electrons and Phonons* (Oxford, New York, 2001).

[41] D. A. McQuarrie, *Statistical Mechanics* (University Science Books, Sausalito, 2000).

[42] A. J. H. McGaughey and M. Kaviany, Physical Review B **69**, 094303 (2004).

[43] J. M. Larkin, J. E. Turney, A. D. Massicotte, C. H. Amon, and A. J. H. McGaughey, to appear in Journal of Computational and Theoretical Nanoscience (2012).

[44] C. J. Morath and H. J. Maris, Phys. Rev. B **54**, 203213 (1996), URL `http://link.aps.org/doi/10.1103/PhysRevB.54.203`.

[45] P. Benassi, M. Krisch, C. Masciovecchio, V. Mazzacurati, G. Monaco, G. Ruocco, F. Sette, and R. Verbeni, Phys. Rev. Lett. **77**, 38353838 (1996), URL `http://link.aps.org/doi/10.1103/PhysRevLett.77.3835`.

[46] S. N. Taraskin and S. R. Elliott, Philosophical Magazine Part B **79**, 17471754 (1999), URL `http://www.tandfonline.com/doi/abs/10.1080/13642819908223057`.

[47] S. N. Taraskin and S. R. Elliott, Phys. Rev. B **61**, 1201712030 (2000), URL `http://link.aps.org/doi/10.1103/PhysRevB.61.12017`.

[48] W. Gtze and M. R. Mayr, Phys. Rev. E **61**, 587606 (2000), URL `http://link.aps.org/doi/10.1103/PhysRevE.61.587`.

[49] G. Ruocco, F. Sette, R. Di Leonardo, G. Monaco, M. Sampoli, T. Scopigno, and G. Viliani, Phys. Rev. Lett. **84**, 57885791 (2000), URL `http://link.aps.org/doi/10.1103/PhysRevLett.84.5788`.

[50] G. Ruocco and F. Sette, Journal of Physics: Condensed Matter **13**, 9141 (2001), URL `http://stacks.iop.org/0953-8984/13/i=41/a=307`.

[51] J. Horbach, W. Kob, and K. Binder, The European Physical Journal B - Condensed Matter and Complex Systems **19**, 531 (2001), ISSN 1434-6028, URL `http://dx.doi.org/10.1007/s100510170299`.

[52] A. Matic, D. Engberg, C. Masciovecchio, and L. Brjesson, Phys. Rev. Lett. **86**, 38033806 (2001), URL `http://link.aps.org/doi/10.1103/PhysRevLett.86.3803`.

[53] J. L. Feldman, Journal of Non-Crystalline Solids **307310**, 128 (2002), ISSN 0022-3093, URL `http://www.sciencedirect.com/science/article/pii/S0022309302014503`.

[54] B. Rufflˆ, M. Foret, E. Courtens, R. Vacher, and G. Monaco, Phys. Rev. Lett. **90**, 095502

(2003), URL http://link.aps.org/doi/10.1103/PhysRevLett.90.095502.

[55] W. Schirmacher, G. Ruocco, and T. Scopigno, Phys. Rev. Lett. **98**, 025501 (2007), URL http://link.aps.org/doi/10.1103/PhysRevLett.98.025501.

[56] J. K. Christie, S. N. Taraskin, and S. R. Elliott, Journal of Non-Crystalline Solids **353**, 2272 (2007), ISSN 0022-3093, URL http://www.sciencedirect.com/science/article/pii/S0022309307002840.

[57] H. Shintani and H. Tanaka, Nat Mater **7**, 870 (2008), ISSN 1476-1122, URL http://dx.doi.org/10.1038/nmat2293.

[58] N. Xu, V. Vitelli, M. Wyart, A. J. Liu, and S. R. Nagel, Phys. Rev. Lett. **102**, 038001 (2009), URL http://link.aps.org/doi/10.1103/PhysRevLett.102.038001.

[59] C. Ganter and W. Schirmacher, Phys. Rev. B **82**, 094205 (2010), URL http://link.aps.org/doi/10.1103/PhysRevB.82.094205.

[60] V. Vitelli, N. Xu, M. Wyart, A. J. Liu, and S. R. Nagel, Phys. Rev. E **81**, 021301 (2010), URL http://link.aps.org/doi/10.1103/PhysRevE.81.021301.

[61] M. Wyart, EPL (Europhysics Letters) **89**, 64001 (2010), URL http://stacks.iop.org/0295-5075/89/i=6/a=64001.

[62] S. Ayrinhac, M. Foret, A. Devos, B. Ruffl, E. Courtens, and R. Vacher, Phys. Rev. B **83**, 014204 (2011), URL http://link.aps.org/doi/10.1103/PhysRevB.83.014204.

[63] J. Callaway, Physical Review **113**, 1046 (1959).

[64] P. G. Klemens, Proceedings of the Physical Society. Section A **68** (1955).

[65] The summation in Eq. (10) is performed over all modes $j \neq i$ including modes $\omega_i < \omega_{cut}$. Excluding modes below the cutoff has an effect only on the modes within the the average mode frequency spacing of ω_{cut}.

[66] A. J. H. McGaughey and M. Kaviany, International Journal of Heat and Mass Transfer **47**, 17831798 (2004).

[67] S. Plimpton, Journal of Computational Physics **117**, 1 19 (1995), ISSN 0021-9991, URL http://www.sciencedirect.com/science/article/pii/S002199918571039X.

[68] B. W. H. van Beest, G. J. Kramer, and R. A. van Santen, Physical Review Letters **64**, 19551958 (1990).

[69] G. J. Kramer, N. P. Farragher, B. W. H. van Beest, and R. A. van Santen, Physical Review B **43**, 50685080 (1991).

[70] Y. Guissani and B. Guillot, The Journal of Chemical Physics **104**, 7633 (1996), URL http://link.aip.org/link/?JCP/104/7633/1.

[71] D. Wolf, P. Keblinski, S. R. Phillpot, and J. Eggebrecht, The Journal of Chemical Physics **110**, 8254 (1999), URL http://link.aip.org/link/?JCP/110/8254/1.

[72] F. H. Stillinger and T. A. Weber, Physical Review B **31**, 52625271 (1985).

[73] U. Buchenau, H. M. Zhou, N. Nucker, K. S. Gilroy, and W. A. Phillips, Phys. Rev. Lett. **60**, 13181321 (1988), URL http://link.aps.org/doi/10.1103/PhysRevLett.60.1318.

[74] M. Durandurdu and D. A. Drabold, Phys. Rev. B **66**, 155205 (2002), URL http://link.aps.org/doi/10.1103/PhysRevB.66.155205.

[75] N. Bernstein, J. L. Feldman, and M. Fornari, Phys. Rev. B **74**, 205202 (2006), URL http://link.aps.org/doi/10.1103/PhysRevB.74.205202.

[76] K. Momma and F. Izumi, Journal of Applied Crystallography **41**, 653658 (2008), URL http://dx.doi.org/10.1107/S0021889808012016.

[77] J. Chen, G. Zhang, and B. Li, Physics Letters A **374**, 23922396 (2010), ISSN 0375-9601, URL http://www.sciencedirect.com/science/article/pii/S0375960110004081.

[78] J. D. Gale and A. L. Rohl, Molecular Simulation **29**, 291 (2003).

[79] D. Donadio and G. Galli, Phys. Rev. Lett. **102**, 195901 (2009).

[80] E. S. Landry and A. J. H. McGaughey, Journal of Applied Physics **107**, 013521 (2010).

[81] F. Sette, M. H. Krisch, C. Masciovecchio, G. Ruocco, and G. Monaco, Science **280**, 1550 (1998), URL http://www.sciencemag.org/content/280/5369/1550.abstract.

[82] B. Ruzicka, T. Scopigno, S. Caponi, A. Fontana, O. Pilla, P. Giura, G. Monaco, E. Pontecorvo, G. Ruocco, and F. Sette, Phys. Rev. B **69**, 100201 (2004), URL http://link.aps.org/doi/10.1103/PhysRevB.69.100201.

[83] D. Kaya, N. L. Green, C. E. Maloney, and M. F. Islam, Science **329**, 656 (2010), URL http://www.sciencemag.org/content/329/5992/656.abstract.

[84] N. L. Green, D. Kaya, C. E. Maloney, and M. F. Islam, Physical Review E **83**, 051404 (2011), URL http://link.aps.org/doi/10.1103/PhysRevE.83.051404.

[85] S. Volz and G. Chen, Physical Review B **61**, 26512656 (2000).

[86] V. Martin-Mayor, M. Mezard, G. Parisi, and P. Verrocchio, The Journal of Chemical Physics **114**, 8068 (2001), URL http://link.aip.org/link/?JCP/114/8068/1.

[87] S. Ciliberti, T. S. Grigera, V. Martin-Mayor, G. Parisi, and P. Verrocchio, The Journal of

Chemical Physics **119**, 8577 (2003), URL http://link.aip.org/link/?JCP/119/8577/1.

[88] Y. M. Beltukov, V. I. Kozub, and D. A. Parshin, Phys. Rev. B **87**, 134203 (2013), URL http://link.aps.org/doi/10.1103/PhysRevB.87.134203.

[89] J. Larkin and A. McGaughey, Journal of Applied Physics (2013).

[90] A. Marruzzo, W. Schirmacher, A. Fratalocchi, and G. Ruocco, Sci. Rep. **3** (2013), URL http://dx.doi.org/10.1038/srep01407.

[91] J. Cowpe, J. Astin, R. Pilkington, and A. Hill, A collection of papers presented at the Euro Mediterranean Symposium on Laser Induced Breakdown Spectroscopy (EMSLIBS 2007) **63**, 1066 (2008), ISSN 0584-8547, URL http://www.sciencedirect.com/science/article/pii/S0584854708002656.

[92] R. Biswas, A. M. Bouchard, W. A. Kamitakahara, G. S. Grest, and C. M. Soukoulis, Phys. Rev. Lett. **60**, 22802283 (1988), URL http://link.aps.org/doi/10.1103/PhysRevLett.60.2280.

[93] J. C. Duda, T. S. English, D. A. Jordan, P. M. Norris, and W. A. Soffa, Journal of Physics: Condensed Matter **23**, 205401 (2011), URL http://stacks.iop.org/0953-8984/23/i=20/a=205401.

[94] Y. He, D. Donadio, J.-H. Lee, J. C. Grossman, and G. Galli, ACS Nano **5**, 18391844 (2011), URL http://pubs.acs.org/doi/abs/10.1021/nn2003184.

[95] Y. He, D. Donadio, and G. Galli, Nano Letters **11**, 3608 (2011), ISSN 1530-6984, URL http://dx.doi.org/10.1021/nl201359q.

[96] T. Hori, T. Shiga, and J. Shiomi, Journal of Applied Physics **113**, 203514 (2013), URL http://link.aip.org/link/?JAP/113/203514/1.

[97] R. Vacher, J. Pelous, F. Plicque, and A. Zarembowitch, Journal of Non-Crystalline Solids **45**, 397 (1981), ISSN 0022-3093, URL http://www.sciencedirect.com/science/article/pii/0022309381900600.

[98] A. Polian, D. Vo-Thanh, and P. Richet, EPL (Europhysics Letters) **57**, 375 (2002), URL http://stacks.iop.org/0295-5075/57/i=3/a=375.

[99] M. D. Kluge and J. R. Ray, Phys. Rev. B **37**, 41324136 (1988), URL http://link.aps.org/doi/10.1103/PhysRevB.37.4132.

[100] J. L. Feldman, J. Q. Broughton, and F. Wooten, Phys. Rev. B **43**, 21522158 (1991), URL http://link.aps.org/doi/10.1103/PhysRevB.43.2152.

[101] F. Wooten, K. Winer, D. Weaire, et al., Physical review letters **54**, 13921395 (1985).

[102] R. Vacher, H. Sussner, and M. Schmidt, Solid State Communications **34**, 279 (1980), ISSN 0038-1098, URL http://www.sciencedirect.com/science/article/pii/0038109880905578.

[103] A. J. C. Ladd, B. Moran, and W. G. Hoover, Physical Review B **34**, 50585064 (1986).

[104] A. S. Henry and G. Chen, Journal of Computational and Theoretical Nanoscience **5**, 112 (2008).

[105] J. E. Turney, E. S. Landry, A. J. H. McGaughey, and C. H. Amon, Phys. Rev. B **79**, 064301 (2009), URL http://link.aps.org/doi/10.1103/PhysRevB.79.064301.

[106] Y. He, I. Savic, D. Donadio, and G. Galli, Phys. Chem. Chem. Phys. p. (2012), URL http://dx.doi.org/10.1039/C2CP42394D.

[107] P. Sheng and M. Zhou, Science **253**, 539542 (1991), URL http://www.sciencemag.org/content/253/5019/539.abstract.

[108] V. Mazzacurati, G. Ruocco, and M. Sampoli, EPL (Europhysics Letters) **34**, 681 (1996), URL http://stacks.iop.org/0295-5075/34/i=9/a=681.

[109] S. R. Bickham and J. L. Feldman, Phys. Rev. B **57**, 1223412238 (1998), URL http://link.aps.org/doi/10.1103/PhysRevB.57.12234.

[110] S. R. Bickham, Phys. Rev. B **59**, 48944897 (1999), URL http://link.aps.org/doi/10.1103/PhysRevB.59.4894.

[111] J. Fabian and P. B. Allen, Phys. Rev. Lett. **77**, 38393842 (1996), URL http://link.aps.org/doi/10.1103/PhysRevLett.77.3839.

[112] J. Fabian, J. L. Feldman, C. S. Hellberg, and S. M. Nakhmanson, Phys. Rev. B **67**, 224302 (2003), URL http://link.aps.org/doi/10.1103/PhysRevB.67.224302.

[113] P. Jund and R. Jullien, Physical Review B **59**, 1370713711 (1999).

[114] S. Shenogin, A. Bodapati, P. Keblinski, and A. J. H. McGaughey, Journal of Applied Physics **105**, 034906 (2009), URL http://link.aip.org/link/?JAP/105/034906/1.

[115] J. Shiomi, K. Esfarjani, and G. Chen, Physical Review B **84**, 125209 (2011).

[116] K. Esfarjani, G. Chen, and H. T. Stokes, Physical Review B **84**, 085204 (2011).

[117] We do not observe that tiling an a-Si model increases the thermal conductivity above the expected linear scaling as was found in Ref. 28 using the MD-based direct method. This finding is likely due to the small model used to perform the tiling in that study (512 atoms), while we use a large model (100,000 atoms).

[118] D. P. Sellan, J. E. Turney, A. J. H. McGaughey, and C. H. Amon, Journal of Applied Physics **108**, 113524 (2010).

[119] Y. K. Koh and D. G. Cahill, Phys. Rev. B **76**, 075207 (2007), URL `http://link.aps.org/doi/10.1103/PhysRevB.76.075207`.